Journal of Pharmaceutical Innovation (2026) 21:112
https://doi.org/10.1007/s12247-025-10348-2

RESEARCH

Enhanced Cytotoxicity of Luteolin Via Optimized Niosomal Delivery System Against MCF-7 Breast Cancer Cells

Nikhil Girase[1] · Rakesh Daude[2] · Kailas Moravkar[1,3] · Shailesh Chalikwar[1] · Ganesh Shevalkar[4] · Bhushan Bhairav[5]

Received: 8 June 2025 / Accepted: 21 December 2025 / Published online: 12 January 2026

Abstract

Purpose >Luteolin, a naturally occurring flavonoid, exhibits potent anticancer activity but is limited by poor aqueous solubility and low oral bioavailability. This study aimed to develop and optimize a niosomal drug delivery system to enhance the solubility, stability, and therapeutic efficacy of luteolin against breast cancer.

Methods Luteolin-loaded niosomes were prepared using the ethanol injection method and lyophilized with 2.5% mannitol as a cryoprotectant. A Central Composite Design (CCD) was used to optimize formulation variables, including the Span 60: cholesterol molar ratio, lipid concentration, and sonication time. The optimized formulation was evaluated for particle size, polydispersity index (PDI), zeta potential, entrapment efficiency, surface morphology (via TEM), drug release behavior, and in vitro cytotoxicity against MCF-7 breast cancer cells.

Results The optimized niosomal formulation demonstrated a mean particle size of 162.67 ± 2.87 nm, PDI of 0.173 ± 0.01, zeta potential of -34.63 ± 1.07 mV, and entrapment efficiency of 87.07 ± 1.69%. TEM confirmed spherical, nanosized particles. XRD analysis revealed reduced crystallinity of luteolin in the formulation, suggesting improved solubility. The in vitro release study showed sustained drug release over 24 h in both simulated gastric (78.26 ± 3.87%) and intestinal (81.13 ± 2.85%) fluids. Cytotoxicity study showed significantly enhanced cytotoxicity across all tested concentrations for luteolin-loaded niosomes compared to pure luteolin (LUT), indicating improved anti-cancer potential.

Conclusion The developed luteolin-loaded niosomal formulation significantly improved the physicochemical properties and anticancer efficacy of luteolin. These findings suggest that niosomal encapsulation is a promising strategy for enhancing the oral bioavailability and therapeutic potential of luteolin in breast cancer treatment.

Keywords Luteolin · Niosomes · Breast cancer · Ethanol injection method · Central composite design

✉ Ganesh Shevalkar
ganeshshevalkar@gmail.com

✉ Bhushan Bhairav
bbhairav@gmail.com

Nikhil Girase
girasenikhil623@gmail.com

Rakesh Daude
rbdaude@gmail.com

Kailas Moravkar
moravkarkailas1985@gmail.com

Shailesh Chalikwar
pharmashailesh@rediffmail.com

[1] Department of Industrial Pharmacy and Quality Assurance, R. C. Patel Institute of Pharmaceutical Education and Research, Shirpur, India

[2] Government Polytechnic, Jalgaon, India

[3] Regeron Inc, Chuncheon-Si, Gangwon-Do, 24232, South Korea, South Korea

[4] Department of Pharmaceutics, Sandip Institute of Pharmaceutical Sciences, Nashik, India

[5] Department of Quality Assurance, NCRD's Sterling Institute of Pharmacy, Nerul, Navi Mumbai, India

Introduction

Luteolin (3,4,5,7-tetrahydroxyflavone) is a naturally occurring flavonoid abundantly found in various fruits, vegetables, and medicinal herbs. It has attracted significant attention due to its potent antioxidant, anti-inflammatory, and anticancer properties [1]. Several studies have demonstrated its efficacy against a wide range of malignancies, including colon, cervical, lung, liver, breast, prostate, skin, and head and neck cancers [2]. The anticancer activity of luteolin has been attributed to mechanisms such as cell cycle arrest, induction of apoptosis, cellular senescence, and inhibition of survival pathways like PI3K/Akt and NF-κB [3]. For instance, luteolin has shown synergistic effects when combined with chemotherapeutic agents such as cisplatin, resulting in enhanced apoptosis and reduced tumor growth in breast and gastric cancer models [4].

While such synergistic outcomes are promising, the current study focuses on luteolin as a standalone therapeutic agent. The rationale originates from its pleiotropic anticancer effects, non-toxic profile, and the need to improve its pharmacokinetic limitations. Luteolin suffers from poor aqueous solubility (~ 50.6 µg/mL) and low oral bioavailability (< 5%), leading to insufficient systemic absorption and therapeutic inefficacy following conventional oral administration [5–7]. Consequently, designing an efficient delivery system is essential to maximize its clinical potential.

To address these issues, various advanced drug delivery systems have been explored, such as co-crystals [5], solid dispersion [8], supersaturable self-nanoemulsifying drug delivery systems (S-SNEDDS) [1, 9], solid lipid nanoparticles (SLNs) [7], nanoemulsions [10], and cyclodextrin inclusion complexes [11]. These approaches have shown improvements in solubility, permeability, and bioavailability of luteolin. However, each system presents limitations: nanoemulsions may suffer from poor long-term stability [12], S-SNEDDS and co-crystals are prone to drug recrystallization [13], SLNs often exhibit low drug loading [14, 15], and cyclodextrin complexes face scalability challenges [16, 17].

In this context, niosomes, a vesicular nanocarrier composed of non-ionic surfactants and cholesterol, emerge as a versatile and scalable alternative. Niosomes have been extensively studied for improving the delivery of hydrophobic drugs due to their ability to encapsulate both hydrophilic and lipophilic agents, protect drug molecules from enzymatic degradation, and prolong circulation time [18, 19]. Compared to liposomes, niosomes offer greater chemical stability, ease of sterilization, lower production cost, and enhanced shelf-life [19]. Notably, in oral drug delivery, niosomes possess multiple advantages like, protection of encapsulated drugs from gastric acid and digestive enzymes due to bilayer structure, enhanced intestinal absorption via endocytosis or transcellular routes due to nanosize, bypass first-pass metabolism to promote lymphatic uptake, and improved therapeutic performance by modifying the release [20]. Examples such as paclitaxel- and griseofulvin-loaded niosomes have shown significantly improved oral bioavailability and pharmacokinetic profiles [21, 22]. Given luteolin's hydrophobic nature and anticancer relevance, particularly in breast cancer, its formulation into niosomes is expected to improve oral delivery, enhance stability, and maximize its therapeutic potential.

In this study, we report the formulation and optimization of luteolin-loaded niosomes using a Central Composite Design (CCD) to systematically study the influence of formulation variables. The developed formulation was evaluated for its physicochemical characteristics, in vitro drug release, and cytotoxic potential against MCF-7 breast cancer cells, an estrogen receptor-positive human breast cancer cell line commonly used to screen anticancer agents [23]. This approach is aimed at developing a scalable, effective, and orally bioavailable niosomal delivery system for luteolin that can be further translated into clinical applications.

Materials and Methods

Materials

Luteolin was generously provided by Sami Labs Ltd., Bengaluru, India. Span 60, cholesterol, mannitol, ethanol (analytical grade), sodium hydroxide, and monobasic potassium dihydrogen phosphate were purchased from Loba Chemie Pvt. Ltd., Mumbai, India. All reagents and solvents used in this study were of analytical grade and used as received.

Formulation of Luteolin-Loaded Niosomes

Luteolin-loaded niosomes were prepared using the ethanol injection method [24]. A lipid phase consisting of Span 60 and cholesterol (at specific molar ratios) was dissolved in 5 mL of ethanol, followed by the addition of 10 mg of luteolin. This resultant clear ethanolic solution was injected slowly using a 22-gauge needle syringe at a controlled rate of 0.5–1.5 mL/min into a preheated 10 mL distilled water maintained at 60 °C under continuous magnetic stirring (Remi Instruments, India) at 500 rpm. The resulting niosomal dispersion was probe-sonicated using a probe sonicator (Dakshin, Mumbai) operated at 40 W for 2 min with an off-time of 3 s to reduce particle size and get a milky white dispersion. Ethanol was removed

under reduced pressure using a rotary evaporator (Buchi Laboratory Equipment, Switzerland). The final volume of niosomal dispersion was maintained at 10 mL, and it was left to mature overnight at 4 °C and stored at refrigerator temperature for further studies.

Optimization of Luteolin-Loaded Niosomes

Before optimizing the luteolin-loaded niosomes, various formulation and process parameters were screened to identify the critical material attributes (CMAs) and critical process parameters (CPPs) influencing the critical quality attributes (CQAs) of the niosomes. The CMAs investigated included concentration of cholesterol, concentration of Span 60, molar ratio of Span 60: cholesterol, and drug concentration, while the CPPs examined comprised sonication time. The CQAs evaluated included the amount of an entrapped drug, particle size, and stability of the niosomes. Following this preliminary screening, a CCD was employed to optimize the formulation and investigate the effects of the CMAs and CPP on the CQAs. The experimental range for each factor was determined based on the results of the preliminary screening experiments. The design details are listed in the supplementary file (Table S1).

CCD was generated using Design Expert software (Version 7.1.6, Stat-Ease Inc., MN) to investigate the effects of CMAs and CPPs on the CQAs of the niosomal formulation. A total of 20 experiments were designed and performed to study the relationships between the variables. The experimental design and corresponding results are presented in Table 1. Analysis of variance (ANOVA) was employed to analyze the statistical significance of the data and identify the most influential factors affecting the CQAs.

Optimization of Design and Model Validation

The experimental data obtained from the 20 designed experiments were analyzed using multiple linear regression to develop a predictive model for the responses. The best-fitting mathematical model was selected based on the highest values of multiple correlation coefficient (R^2), adjusted R^2, and predicted residual sum of squares (PRESS), as well as the lowest coefficient of variation (CV). The significance of the model was evaluated at a probability level of $p < 0.05$. Three-dimensional response surface curves and two-dimensional overlay plots were generated using the Design Expert software to visualize the relationships between the independent variables and the responses. These plots facilitated the identification of the optimal formulation conditions and the prediction of the corresponding response values.

Physicochemical Characterization

The developed niosomes were characterized with respective to physicochemical properties like particle size, zeta potential, surface morphology, entrapment efficiency (% EE), solid-state characterization (IR, and XRD), in vitro drug release, and in vitro cytotoxicity.

Table 1 CCD design and responses for luteolin-loaded niosome optimization

Batch no.	(X_1) Span 60: Cholesterol ratio	(X_2) Lipid conc. (mg)	(X_3) Sonication Time (min)	(Y_1) Particle size (nm)	(Y_2) Zeta potential (mV)	(Y_3) EE (%)
1	0.16	300	4	241	−35.9	89.3
2	1	300	4	185.3	−36.3	81.86
3	1.5	400	2	169.9	−38.9	83.44
4	0.5	200	2	214.8	−33.9	82.78
5	0.5	400	2	202.1	−37.3	83.22
6	1.84	300	4	211.6	−37.6	82.56
7	1	300	7.4	208.9	−33.3	86.72
8	1	131.82	4	188.5	−41.7	76.39
9	0.5	200	6	314	−32.7	79.64
10	1.5	200	2	247	−39.6	71.12
11	1	300	4	157.5	−36.2	83.79
12	1	300	4	195.7	−38.3	82.49
13	1.5	400	6	236	−27.8	82.97
14	1	300	4	208.9	−41.39	84.45
15	1	300	4	219.8	−42.3	86.97
16	1	468.18	4	1414	−40.6	79.84
17	0.5	400	6	1190	−31.1	76.21
18	1	300	0.6	235.5	−36.1	79.65
19	1	300	4	216.8	−33.6	80.26
20	1.5	200	6	206.6	−32.2	75.59

Span 60: cholesterol ratios are expressed as molar values (1 = 1:1, 0.5 = 0.5:1, 1.5 = 1.5:1)

Particle Size, Polydispersity Index (PDI), and Zeta Potential Analysis

The particle size, polydispersity index (PDI), and zeta potential of the luteolin-loaded niosomes were determined using a Malvern Zetasizer (Nano ZS 90, Malvern Ltd., UK) based on the principle of dynamic light scattering (DLS). Prior to analysis, the niosomal formulations were diluted 1:100 with double-distilled water. This dilution was performed to ensure the sample concentration was within the optimal range for DLS analysis, minimizing multiple scattering effects and ensuring accurate measurement of particle size, PDI, and zeta potential. The measurements were carried out at 25 ± 1 °C in triplicate, and the mean values were reported [25].

The zeta potential, which measures the electrostatic charge on the surface of the particles, was determined by evaluating the electrophoretic mobility using the same instrument. This analysis provided valuable insights into the surface properties and stability of the luteolin-loaded niosomes.

Transmission Electron Microscopy (TEM)

The morphology and structure of the optimized luteolin-loaded niosomes were examined using a transmission electron microscope (Morgagni 268D, FEI, USA) operated at an accelerating voltage of 100 kV. A suitably diluted dispersion of the niosomes was placed on a 400-mesh carbon film-coated copper grid. The grid was stained with 1% phosphotungstic acid for 10 s to enhance contrast. The TEM images provided valuable information on the size, shape, and morphology of the optimized niosomal formulation [26].

Entrapment Efficiency (% EE)

The % EE of luteolin in niosomes was determined using the dialysis bag method [27]. A measured amount of drug-loaded niosomal formulation was placed in a dialysis bag (12 kDa molecular weight cut-off, Thermo Scientific, Waltham, MA, USA) and immersed in a dialysis medium. At predetermined time intervals up to 4 h, samples were collected from the external dialysis medium, and the free drug content was analyzed using a UV-visible spectrophotometer (UV 1700, Shimadzu, Japan). The % EE of luteolin in niosomes was calculated using the following equation:

$$\%\,\mathrm{EE} = \frac{Amount\ of\ luteolin\ added - Amount\ of\ luteolin\ in\ media}{Amount\ of\ luteolin\ added} \times 100$$

Solid-State Characterization of Niosomes

To confirm the encapsulation of luteolin within the niosomal particles, solid-state characterization techniques like X-ray diffraction and FTIR analysis were performed. As these techniques require the sample in solid form, the luteolin-loaded niosomes were freeze-dried specifically for this purpose. Prior to analysis, the luteolin-loaded niosomes were freeze-dried (Freeze dryer, Ad Vantage EL, Virtis SP Scientific, USA) using 2.5% mannitol as a cryoprotectant to preserve the structural integrity of the niosomes during the drying process. This allowed accurate assessment of crystallinity and drug–excipient interactions without compromising particle morphology.

X-ray Diffraction (XRD)

The crystalline structures of pure luteolin, blank niosomes, and freeze-dried luteolin-loaded niosomes were investigated using an X-ray diffractometer (Bruker D2 Phaser 2nd Gen, Germany). The samples were mounted on a sample holder and subjected to XRD analysis. The diffraction patterns were recorded over a 2θ range of 5°–60°, with a scan rate of 5°/min, using a voltage of 40 kV and a current of 100 mA. The XRD analysis was performed on the following samples: (1) pure luteolin, (2) blank niosomes, and (3) freeze-dried luteolin-loaded niosomes [5].

Fourier Transform Infrared (FTIR) Spectroscopy

FTIR spectrum of luteolin was recorded using a FTIR spectrophotometer (Shimadzu 8400 S, Japan). A pellet of luteolin was prepared by mixing the compound with IR-grade potassium bromide (KBr) in a 1:100 ratio. The mixture was compressed into a 13 mm diameter disk and scanned over a wavenumber range of 4000–400 cm^{-1}. The resulting FTIR spectrum was analyzed to identify the characteristic absorption peaks of luteolin [28].

Drug-excipient Interaction Study

A drug-excipient interaction study was conducted to investigate potential interactions between luteolin and the excipients used in the formulation. A physical mixture of luteolin and excipients was prepared in an amber-colored glass vial and stored under accelerated stability conditions (40 ± 2 °C and 75 ± 5% RH) for a period of 4 weeks. After storage, the samples were analyzed using FTIR spectroscopy to detect any changes in the spectral patterns, indicating potential interactions between the drug and excipients [29].

In Vitro Drug Release

The in vitro drug release behavior of the optimized luteolin-loaded niosomes was analyzed using the dialysis bag diffusion method [30]. Release studies were carried out in two

media: simulated gastric fluid (SGF, pH 1.2), prepared using 0.1 M HCl, and simulated intestinal fluid (SIF, pH 6.8), prepared using phosphate buffer. Because luteolin has limited aqueous solubility, 1.5% w/v hydroxypropyl-β-cyclodextrin (HP-β-CD) was added to each release medium to maintain proper sink conditions. HP-β-CD enhances luteolin solubility through inclusion-complex formation without generating micelles, thereby preventing membrane pore blockage and eliminating the risk of local supersaturation or drug precipitation. This modification ensures reliable sink conditions and a more accurate evaluation of release behavior. Prior to use, the dialysis membrane (MWCO ~ 12–14 kDa, HiMedia, India) was activated by soaking in double-distilled water for 12 h to remove glycerine and preservatives, followed by thorough rinsing to ensure uniform permeability. The dialysis bag containing the niosomal formulation was immersed in the respective release medium and maintained at 37 ± 0.5 °C under continuous stirring. At predetermined time intervals (2, 4, 8, 12, 18, and 24 h), 5 mL of the release medium was collected and replaced with an equal volume of fresh medium. The collected samples were filtered, appropriately diluted, and analyzed for luteolin content at 268 nm using a UV spectrophotometer.

In Vitro Cytotoxicity

The cytotoxicity of the developed formulation was evaluated in vitro using the MCF-7 human breast cancer cell line, obtained from the National Centre for Cell Science (NCCS), Pune, India [31]. The cells were cultured in Dulbecco's Modified Eagle Medium (DMEM) (high glucose, Cat. No. 11965-092), supplemented with 10% fetal bovine serum (FBS) and 1% penicillin/streptomycin. The cell line was maintained in 25 cm^2 culture flasks at 37 °C in a humidified atmosphere containing 5% CO_2 until ~ 80% confluency was achieved. Upon reaching the desired confluency, the cells were trypsinized, followed by centrifugation at 1300 × g for 7 min. The pellet was then re-suspended in fresh culture medium. Cells were counted using a hemocytometer and seeded in 96-well tissue culture plates at a density of 1×10^4 cells/well in 100 µL of culture medium. The plates were incubated for 24 h at 37 °C in a 5% CO_2 incubator (Thermo Scientific BB150) to allow cell attachment [32].

After incubation, different volumes (10, 40, and 100 µL) of the test formulation were added to the respective wells [33]. Control wells received 0.2% DMSO in PBS. Post-treatment, the plates were incubated for another 24 h under the same conditions. Following exposure, the medium was removed and replaced with 20 µL of MTT reagent (5 mg/mL in PBS) in each well. The plates were incubated for 4 h to allow the formation of purple formazan crystals. After incubation, 85 µL of the supernatant was carefully removed from each well, and 50 µL of DMSO was added to dissolve the formazan crystals. The contents were pipetted up and down gently to ensure complete solubilization, followed by a 10 min incubation at 37 °C. Finally, the absorbance was measured at 550 nm using a microplate reader. The percentage of cell viability was calculated by comparing the absorbance of treated wells with that of the untreated control group. The IC_{50} value (the concentration of formulation that inhibits 50% of cell proliferation) was determined using dose–response curve fitting [34].

Stability Study

The optimized luteolin-loaded niosomal dispersion was subjected to stability evaluation in accordance with ICH Q1A (R2) guidelines. The dispersion was aseptically filled into clean, sterile amber glass vials, sealed with rubber stoppers, and crimped with aluminium caps to ensure an airtight closure and minimize light exposure. The sealed vials were stored under the refrigerated (4 °C ± 2 °C) and Accelerated (40 °C ± 2 °C/75% ± 5% RH) conditions. The stability study was conducted for a duration of three months. Samples were withdrawn at predetermined time intervals: 0 (initial), 1 month, and 3 months. At each time point, the samples were evaluated for particle size, PDI, zeta potential, entrapment efficiency and drug content. All measurements were performed in triplicate, and results were expressed as mean ± standard deviation.

Statistical Analysis

All experiments were carried out in triplicate ($n = 3$) unless otherwise specified. Data are presented as mean ± standard deviation (SD). Sample size ($n = 3$) was selected based on standard practice in preliminary formulation and cytotoxicity studies to provide sufficient statistical power while maintaining experimental feasibility. Statistical analyses were performed using one-way/two-way ANOVA followed by Tukey's post hoc test for comparisons among multiple groups, and Student's t-test for pairwise comparisons. A p-value < 0.05 was considered statistically significant. Design Expert® software (version 12.03.0, Stat-Ease Inc., Minneapolis, MN) was used for the statistical analysis of data.

Results

Formulation of Luteolin-Loaded Niosomes

The ethanol injection method was selected for the preparation of luteolin-loaded niosomes due to its simplicity, reproducibility, and suitability for large-scale production. This

method supports the fabrication of vesicular systems with controlled particle size and enhanced encapsulation efficiency. Ethanol acts as an efficient solvent for both the active compound and formulation excipients, contributing to particle formation by increasing the bilayer's fluidity during self-assembly [35]. Span 60, a non-ionic surfactant, was utilized owing to its elevated phase transition temperature (~ 53 °C), which aids in producing structurally stable niosomes. Its critical packing parameter (CPP), ranging between 0.5 and 1, and hydrophilic-lipophilic balance (HLB) value near 4.7, favor the formation of spherical particles with reduced drug leakage and improved drug entrapment [36]. Additionally, cholesterol was incorporated into the formulation to reinforce the bilayer's rigidity and mechanical strength, which further supports particle integrity and minimizes the risk of drug leakage [37].

Optimization of Luteolin-Loaded Niosomes

The optimization of critical formulation parameters—zeta potential (stability indicator), particle size, and % EE was performed using a CCD. Among the various experimental designs available, CCD was selected due to its widespread application and efficiency in reducing the number of experimental runs compared to a traditional three-level full factorial design. This design framework includes three key components: (a) factorial design points, (b) axial points, and (c) center points.

A total of 20 experimental runs were generated using CCD, and the corresponding responses are presented in Table 1. The observed ranges for the three dependent variables were as follows: zeta potential from −42.3 to −27.8 mV, particle size from 157.5 to 1414 nm, and % EE from 71.12% to 89.3%. Model selection for response analysis was guided by the sequential model sum of squares, lack-of-fit tests, and model summary statistics. The significance of each variable's effect on the responses was determined using analysis of variance (ANOVA). The analysis revealed that lipid concentration, surfactant-to-cholesterol ratio, and sonication time significantly influenced particle size. In contrast, cholesterol concentration was identified as the critical factor affecting both zeta potential and %EE.

The mathematical equation for responses Y1, Y2, and Y3 are as follows:

$$Y_1\,(Particle\ Size) = +199.99 - 81.34^{*}A + 210.64^{*}B + 78.21^{*}C - 113.87^{*}A^{*}B - 132.68^{*}A^{*}C + 124.40^{*}B^{*}C - 7.13^{*}A2 + 196.14^{*}B2 - 8.58^{*}C2$$

$$Y_2\,(Zeta\ Potential) = -37.74 - 0.1 - 0.47^{*}A + 0.38^{*}B + 10.44^{*}C + 0.86^{*}A^{*}B + 1.39^{*}A^{*}C + 1.09^{*}B^{*}C - 1.34^{*}A2 - 2.89^{*}B2 + 11.16^{*}C2$$

$$Y3\,(\%EE) = +83.40 - 1.47^{*}A + 1.65^{*}B + 0.42^{*}C + 2.84^{*}A^{*}B + 1.77^{*}A^{*}C - 1.10^{*}B^{*}C + 0.30^{*}A2 - 2.46^{*}B2 - 0.67^{*}C2$$

The relationship between CMAs and CQAs was further analyzed using regression coefficients. A negative sign in the regression equation indicates an inverse relationship between the variables, whereas a positive sign reflects a synergistic effect.

For response Y_1 (particle size), an increase in lipid concentration resulted in a corresponding increase in particle size, indicating a positive correlation. Conversely, the negative coefficient for sonication time suggested that higher sonication durations led to a reduction in particle size. In the case of Y_2 (zeta potential), the negative coefficient for cholesterol concentration indicated that an increase in cholesterol up to an optimal level enhanced the stability of the niosomes, as reflected by a more negative zeta potential. Regarding Y_3 (% EE), a decrease in cholesterol concentration led to a decline in %EE, confirming the importance of cholesterol in particle integrity and drug loading. Three-dimensional response surface plots (Fig. 1A) illustrate the combined effects of the independent variables (A: cholesterol concentration, B: Span 60: cholesterol ratio, and C: sonication time) on the measured responses. Figure 1A **(a & b)** show that particle size increased with rising Span 60: cholesterol ratios and lipid concentrations. Figure 1A **(c & d)** depict the zeta potential trends, where the maximum stability (most negative zeta potential) was observed at a Span 60: cholesterol ratio of 1 and a lipid concentration of 300 mg. Deviation from these optimal values in either direction led to reduced zeta potential values, indicating decreased stability.

Figure 1 A (e & f) illustrates the influence on %EE. As the Span 60: cholesterol ratio increased beyond 1, a decline in %EE was observed. Lipid concentration at 200 mg showed a slight negative effect, while at the optimal level of 300 mg, it demonstrated a positive effect. However, further increases in lipid concentration beyond 300 mg led to a gradual decline in %EE.

The Design-Expert® software's point prediction optimization tool was employed to generate the overlay plot (Fig. 1B**)** and derive the optimized formulation based on the defined criteria: minimum particle size, maximum zeta potential (for enhanced stability), and highest possible %EE. The optimized formulation was then experimentally validated. The observed experimental values closely matched the predicted values, confirming the reliability and accuracy of the CCD model (Table S2, Supplementary File). Thus, the CCD was successfully validated for the optimization of the luteolin-loaded niosomal formulation.

Particle Size, PDI, and Zeta Potential Analysis

Particle size is a critical parameter in niosomal formulations, as it significantly influences drug release, permeation, and absorption. Smaller particles offer a larger surface area,

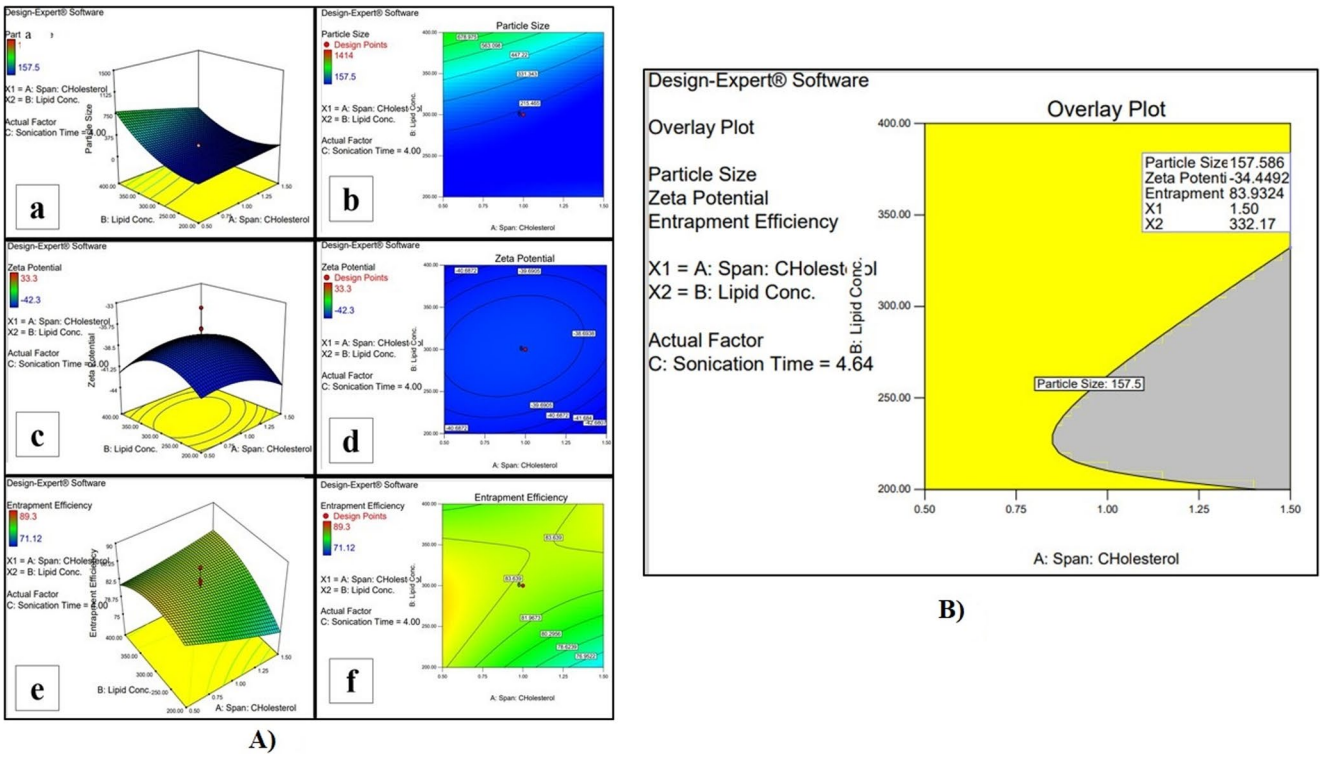

Fig. 1 **A**: Response surface and contour plots showing the effects of Span 60:cholesterol ratio (X_1), lipid concentration (X_2), and sonication time (X_3) on (**a**, **b**) particle size, (**c**, **d**) zeta potential, and (**e**, **f**) entrapment efficiency of luteolin-loaded niosomes. **B:** Overlay plot showing the optimized formulation region (yellow) based on minimized particle size and zeta potential, and maximized entrapment efficiency.

Table 2 Particle size, PDI, zeta potential, and entrapment efficiency of optimized luteolin-loaded niosomes

Particle size (nm)	PDI	Zeta potential (mV)	Entrapment efficiency (%)
162.67 ± 2.87	0.173 ± 0.01	−34.63 ± 1.07	87.07 ± 1.69

Data are presented as mean ± SD (n = 3)

which can enhance mucosal interaction and improve drug absorption, ultimately contributing to better bioavailability. Additionally, the PDI serves as an indicator of the homogeneity of particle size distribution; lower PDI values reflect more uniform and stable formulations [38].

As shown in Table 2, the optimized luteolin-loaded niosomes exhibited a mean particle size of 162.67 ± 2.87 nm, with a PDI of 0.173 ± 0.01, indicating a narrow and uniform size distribution. The %EE was found to be 87.07 ± 1.69%, suggesting effective encapsulation of the drug within the particles. The zeta potential was measured at −34.63 ± 1.07 mV, signifying good colloidal stability due to sufficient surface charge repulsion between particles. The influence of independent formulation variables on particle size was further visualized through three-dimensional response surface and contour plots, as presented in Fig. 1A (a & b).

The particle size below 200 nm is considered ideal for oral drug delivery, as such particles can enhance intestinal uptake via endocytosis or passive diffusion mechanisms. The narrow PDI (<0.2) indicates high uniformity, which reduces the likelihood of particle aggregation and ensures consistent pharmacokinetics. The negative zeta potential of −34.63 mV further contributes to the electrostatic repulsion between particles, minimizing aggregation and enhancing the physical stability of the formulation over time. These attributes collectively indicate that the optimized formulation has favorable physicochemical properties suitable for enhancing the oral bioavailability of luteolin. Moreover, the high entrapment efficiency suggests strong affinity of the hydrophobic drug for the lipid bilayer of the niosomes, likely supported by the appropriate Span 60: cholesterol ratio used in formulation.

Transmission Electron Microscopy (TEM)

The morphology and internal structure of the optimized niosomes was examined using TEM. As depicted in Fig. 2, the particles appeared spherical with smooth, well-defined edges, confirming uniform morphology. The particle size observed via TEM was approximately 100 nm, which was slightly smaller than the size determined by DLS using a Zetasizer [39].

This variation in size measurement can be attributed to the fundamental differences in the analytical techniques. The Zetasizer measures the hydrodynamic diameter of particles

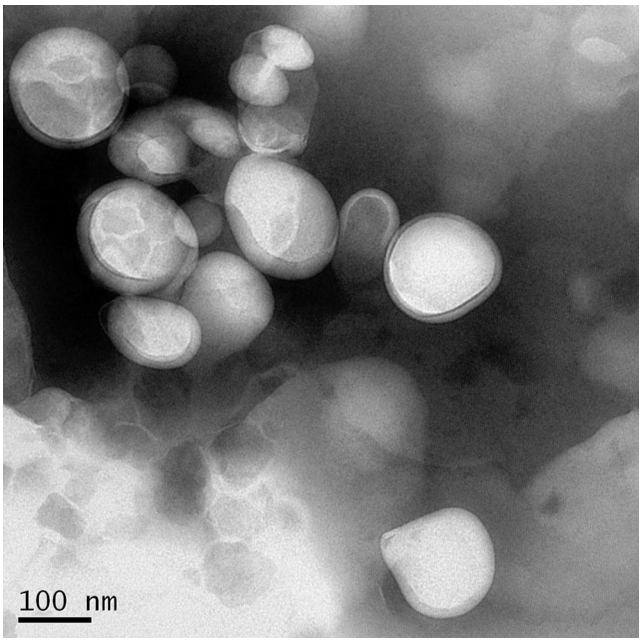

Fig. 2 TEM image of optimized luteolin-loaded niosomes showing spherical morphology and uniform vesicular structure

in their hydrated, dispersed state, including the solvation layer surrounding each particle. In contrast, TEM provides the size of the dried particles under vacuum conditions, thereby yielding a smaller apparent diameter. Despite this difference, the TEM findings support the nanometric size range and uniformity of the formulation observed through DLS analysis [40].

Entrapment Efficiency

The %EE of luteolin-loaded niosomes, prepared using Span 60 and cholesterol, was observed to range from 71.12% to 89.3%. Among the critical formulation components, cholesterol concentration was found to significantly influence the %EE. As illustrated in Fig. 1A (e & f), varying the molar ratio of Span 60 to cholesterol impacted the ability of the niosomes to encapsulate luteolin. The optimized formulation exhibited a high %EE of 87.07 ± 1.69% at a 1:1 molar ratio of Span 60 to cholesterol.

Cholesterol plays a crucial role in the structural and functional stability of niosomal vesicles. As a key membrane component, cholesterol integrates into the bilayer and enhances its rigidity and mechanical strength, thereby maintaining vesicle integrity and preventing drug leakage. This stabilizing effect contributes to improved drug entrapment by minimizing vesicle disruption during preparation and storage. Additionally, the ordered arrangement of surfactant and cholesterol molecules facilitates efficient drug partitioning into the vesicular bilayers [41].

However, while an optimal cholesterol concentration enhances %EE, excessive cholesterol may disrupt the bilayer arrangement. Beyond a certain threshold, increased cholesterol content can interfere with the regular packing of surfactant molecules, destabilizing the vesicular structure and ultimately leading to reduced drug entrapment [42]. Therefore, careful optimization of the Span 60: cholesterol molar ratio is essential to achieve a stable formulation with high %EE. Similar findings were observed in thiocolchcoside loaded niosomal system where concentration of cholesterol and molar ratio of Span 60 and cholesterol play an important role in the encapsulation of thiocolchicoside [43].

X-ray Diffraction

X-ray diffraction (XRD) analysis was performed to evaluate the crystalline nature of luteolin before and after encapsulation within the niosomal vesicles. This study also aimed to confirm the successful incorporation of the drug and any changes in its physical state upon formulation.

Figure 3 presents the XRD patterns of pure luteolin, freeze-dried luteolin-loaded niosomes, and blank niosomes. The diffractogram of pure luteolin revealed sharp, intense peaks at 2θ values of 8.77°, 10.17°, 17.21°, and 25.64°, indicating its crystalline nature. In contrast, these characteristic crystalline peaks of luteolin were absent in the XRD pattern of the freeze-dried drug-loaded niosomes, suggesting a loss of crystallinity and possible conversion to an amorphous or molecularly dispersed state upon encapsulation [8].

The XRD pattern of blank niosomes displayed broad peaks of low intensity, which were also observed in the freeze-dried formulation, albeit with slight shifts and reduced intensities. This reduction in peak sharpness and intensity is indicative of the presence of amorphous or semi-crystalline components such as Span 60 and cholesterol. The disappearance of luteolin characteristic peaks in the niosomal formulation confirms the successful entrapment of the drug within the vesicles and suggests a reduction in crystallinity, which could potentially enhance solubility and bioavailability [44]. Similar findings have been reported by Akbari et al. (2021) for diclofenac-loaded niosomal systems [45].

FTIR-spectroscopy

The FTIR spectrum of luteolin was recorded using the KBr disk method over a scanning range of 4000–400 cm^{-1} with a resolution of 1 cm^{-1}. The resulting spectrum is presented in Figure S1, and the corresponding characteristic peaks are summarized in Table S3 (Supplementary File).

The FTIR analysis of luteolin revealed a strong carbonyl (C = O) stretching band at 1611.80 cm^{-1}, indicative of the ketone functional group. The absence of C–H

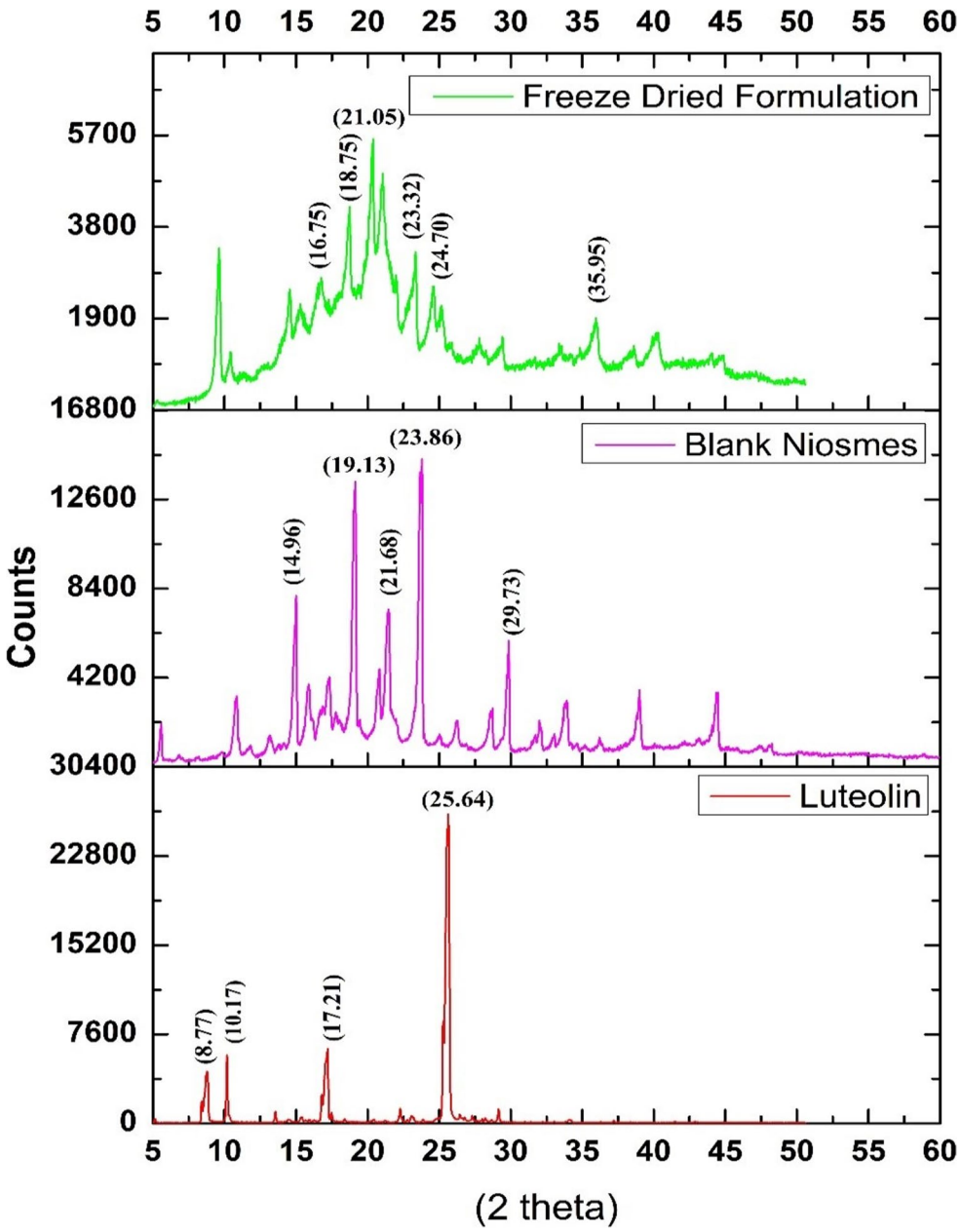

Fig. 3 XRD patterns of pure luteolin, freeze-dried luteolin-loaded niosomes, and blank niosomes

stretching in this region confirmed that the carbonyl group is not part of an aldehyde, thus clearly distinguishing the ketone structure in luteolin. A broad O–H stretching band appeared at 3419.35 cm^{-1}, shifted from the typical alcohol O–H range (~ 3600 cm^{-1}), which is attributed to the hydrogen bonding and resonance effects within the aromatic ring system. This shift is consistent with the presence of phenolic hydroxyl groups, thereby confirming the phenolic structure of luteolin. Additionally, C–O stretching vibrations characteristic of ether functionalities were observed at 1031.03 cm^{-1}, while aromatic C = C stretching bands appeared at 1499.89 cm^{-1}, further supporting the presence of the aromatic framework in the molecule [46].

The FTIR spectra of Span 60 and cholesterol were also recorded to ensure the compatibility of the excipients with the drug. Their respective spectra are shown in **Figures S2 and S3**, and the key characteristic peaks are listed in **Tables S4 and S5**. No significant shifts or disappearance of peaks were observed in the physical mixture, indicating no major interaction between luteolin and the excipients at the molecular level. Similar findings were also reported by Zaid Alkilani et al. for azithromycin loaded niosomes [47].

Drug-Excipient Interaction Study

A drug–excipient interaction study was conducted to evaluate any potential physical or chemical incompatibilities between luteolin and the selected formulation excipients. Such compatibility assessments are essential to ensure the stability, efficacy, and safety of the final dosage form. This study also provides critical insights during the formulation development phase.

The physical mixture of luteolin with the excipients (Span 60 and cholesterol) was prepared and stored under accelerated conditions as per ICH guidelines (Q1A[R2])—specifically at 40 ± 2 °C and 75 ± 5% relative humidity—for a period of four weeks. At the end of the storage period, the samples were subjected to Fourier Transform Infrared (FTIR) spectroscopy to detect any possible interactions at the molecular level.

The FTIR spectrum of pure luteolin exhibited prominent characteristic bands, including a carbonyl (C = O) stretching band at 1611.80 cm^{-1}, a broad O–H stretching band at 3419.35 cm^{-1} (indicative of phenolic hydroxyl groups), an ether (C–O–C) stretching band at 1031.03 cm^{-1}, and an aromatic C = C stretching band at 1499.89 cm^{-1}. All these characteristic peaks were found to be present and unaltered in the FTIR spectrum of the luteolin–excipient physical mixture, as shown in Supplementary Figure S4.

The retention of these functional group peaks in the physical mixture indicates the absence of significant chemical interactions between the drug and excipients during the storage period. These findings confirm the compatibility of luteolin with Span 60 and cholesterol, supporting their suitability for further development of a stable niosomal formulation [5].

In Vitro Drug Release

The in vitro drug release profile of luteolin-loaded niosomes was evaluated in simulated gastric fluid (SGF, pH 1.2) and simulated intestinal fluid (SIF, pH 6.8) to replicate the physiological conditions encountered following oral administration. To maintain appropriate sink conditions and overcome the poor aqueous solubility of luteolin, both media were supplemented with 1.5% w/v hydroxypropyl-β-cyclodextrin (HP-β-CD). The cumulative drug release profiles are shown in Figs. 4 and 5.

In both media, pure luteolin exhibited a rapid and almost complete release, confirming that the presence of HP-β-CD successfully maintained true sink conditions and enabled complete solubilization of the drug throughout the release period. This ensured reliable assessment of the release behavior of the niosomal formulation relative to the pure drug.

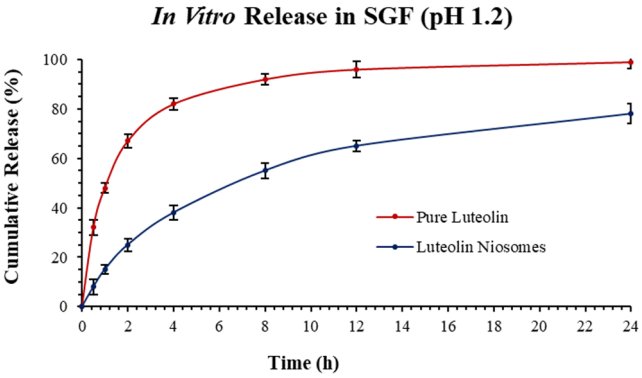

Fig. 4 Drug release profile of pure luteolin and luteolin-loaded niosomes in SGF (pH 1.2)

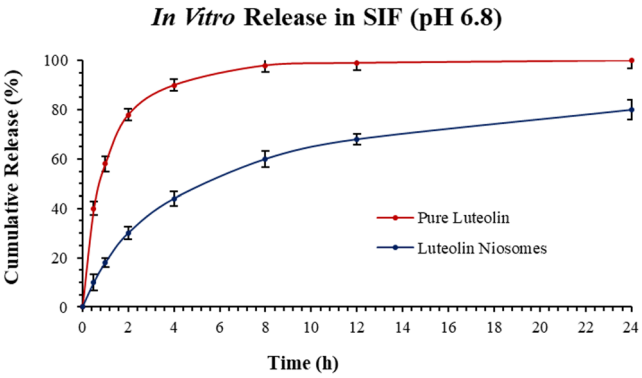

Fig. 5 Drug release profile of pure luteolin and luteolin-loaded niosomes in SIF (pH 6.8)

In contrast, the luteolin-loaded niosomes demonstrated a sustained and controlled release pattern. In SGF (pH 1.2), approximately 78–82% of luteolin was released over 24 h, whereas in SIF (pH 6.8), the cumulative release was approximately 80–85% at the same time point. The slower release of luteolin from the vesicles can be attributed to the rigid and highly ordered bilayer structure formed by Span 60. Its high phase transition temperature supports the formation of stable vesicles with limited permeability, thereby restricting the rapid diffusion of the encapsulated drug [48]. Similar findings have also been reported by Jain et al. for the pilocarpine hydrochloride-loaded niosomes [49].

To explain the drug release mechanism, the release data were fitted into various kinetic models. As shown in Table 3, kinetic modeling gave clearer insight into how the formulations behaved during the release study.

Pure luteolin showed a strong fit to the first-order model ($R^2 \approx 0.958$), confirming that its release was mainly concentration-dependent and occurred rapidly. In contrast, the niosomal formulation best aligned with the Higuchi ($R^2 \approx 0.960$) and Korsmeyer–Peppas ($R^2 \approx 0.960$) models. This shift toward diffusion-controlled

Table 3 Drug release kinetics of pure Luteolin and Luteolin-loaded niosomes in SGF (pH 1.2) and SIF (pH 6.8)

Parameter	SGF (pH 1.2)		SIF (pH 6.8)	
	Pure Luteolin	Luteolin-loaded niosomes	Pure Luteolin	Luteolin-loaded niosomes
Zero-order (R^2)	0.521	0.830	4.425	0.787
First-order (R^2)	0.933	0.948	0.958	0.928
Higuchi (R^2)	0.791	0.975	0.704	0.960
Korsmeyer–Peppas (R^2)	0.891	0.970	0.842	0.960
n- value	0.288	0.592	0.229	0.538
Best-fit Model	First-order	Higuchi/Peppas	First-order	Higuchi/Peppas

kinetics is common for vesicular delivery systems and indicates that luteolin is released gradually as it diffuses through the hydrated surfactant layers of the niosomes.

The n value obtained from the Korsmeyer–Peppas model further clarifies the release mechanism. Pure luteolin exhibited an n value of approximately 0.23, indicative of Fickian diffusion, where drug release is driven predominantly by passive diffusion into the surrounding medium. On the other hand, luteolin-loaded niosomes exhibited an n value of around 0.54, reflecting non-Fickian (anomalous) diffusion. This means that drug release is influenced not only by diffusion but also by structural relaxation or reorganization of the niosomal bilayer, an expected behavior in lipid-based nanocarriers as they hydrate and interact with the medium. Overall, the niosomal system successfully extended the release of luteolin over 24 h and prevented any substantial initial burst release. These findings confirm that the sustained release of luteolin from niosomes is governed by both diffusion of drug molecules through the vesicle bilayer and matrix relaxation or erosion over time. Such release behavior is desirable for oral administration, where prolonged drug availability can improve bioavailability and therapeutic outcomes [50].

In Vitro Cytotoxicity

The cytotoxic potential of luteolin-loaded niosomes was assessed in vitro using the MTT assay against the MCF-7 human breast cancer cell line, with comparisons made to pure luteolin and the standard chemotherapeutic agent, 5-fluorouracil (5-FU). As shown in Fig. 6, all test samples exhibited a concentration-dependent reduction in cell viability. Notably, luteolin-loaded niosomes (N-LUT) demonstrated significantly enhanced cytotoxicity across all concentrations tested (10, 40, and 100 µg/mL) compared to pure luteolin (LUT), indicating improved anti-cancer potential [33, 51].

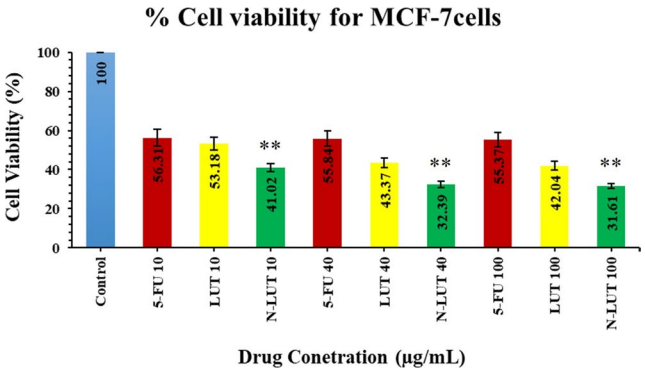

Fig. 6 Percentage cell viability of MCF-7 cells after treatment with luteolin and luteolin-loaded niosomes (10, 40, and 100 µg/mL). Where, $^{**}p<0.01$

Quantitative analysis revealed that the IC_{50} value for niosomal luteolin was 25.76 µg/mL, significantly lower than that of pure luteolin (50.08 µg/mL) and comparable to 5-FU (21.91 µg/mL). Two-way ANOVA followed by Tukey's post hoc test confirmed statistically significant differences between free and niosomal luteolin ($P < 0.01$), supporting the enhanced cytotoxic effect imparted by the niosomal delivery system.

However, further evidence of anti-proliferative activity was provided by morphological examination using an inverted phase-contrast microscope **(**Fig. 7**).** MCF-7 cells treated with luteolin-loaded niosomes exhibited prominent features of apoptosis, including cell shrinkage, rounding, detachment from the surface, and an increased number of floating cells. These observations suggest that the niosomal formulation not only improves drug delivery but also effectively induces apoptotic cell death. The enhanced cytotoxic effect of the niosomal luteolin may be attributed to multiple mechanisms, including increased cellular uptake, sustained intracellular drug release, and the activation of apoptosis pathways [52]. Similar finding has also been reported by Barani M. et al. for thymoquinone [53] and lawsone [54] loaded niosomes where improved activity of thymoquinone and lawsone were observed against MCF-7 breast cancer cell line when these molecules has been administered in the form of niosomes.

While direct mechanistic assays such as apoptosis markers, ROS generation, and caspase activity were not conducted in the present study, literature evidence suggests that luteolin and its nanoformulations exert anticancer activity through these pathways, including activation of caspase enzymes [55], regulation of reactive oxygen species (ROS) [56], DNA damage induction, and inhibition of oncogenic protein kinases [52]. These mechanisms have been reported to contribute synergistically to the suppression of cancer cell proliferation, angiogenesis, and metastasis [44]. In this work, the enhanced cytotoxicity and morphological changes observed with luteolin-loaded niosomes are consistent with these reported mechanisms, although further mechanistic validation will be required.

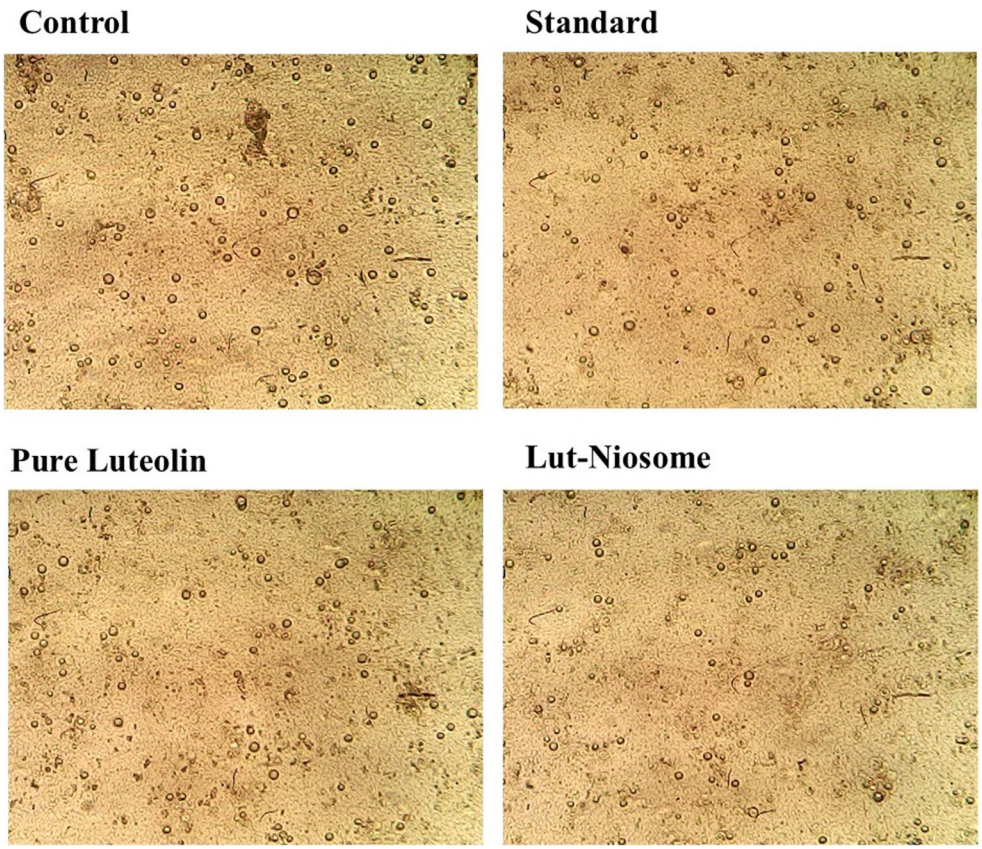

Fig. 7 Morphological changes in MCF-7 cells under control, 5-fluorouracil, luteolin, and niosomal luteolin treatments (magnification = 20×)

In a broader context, it is also important to compare the performance of niosomes with clinically relevant nanocarriers. Liposomes, while clinically established, are often limited by oxidative instability and high production cost [57]. Polymeric nanoparticles offer controlled release but involve complex synthesis and potential toxicity concerns [58]. Polymeric micelles are effective solubilizers but may suffer from premature drug release [59], while dendrimers, despite their structural precision, face scalability and cytotoxicity challenges [60, 61]. In contrast, the optimized luteolin-loaded niosomes in this study combined favorable stability, high entrapment efficiency, and enhanced cytotoxicity, highlighting their potential as a cost-effective and scalable alternative. Nonetheless, as with all nanocarriers, in vivo studies remain essential for translational validation. Taken together, the current findings provide preliminary biological evidence supporting the therapeutic potential of the optimized formulation, which warrants more detailed mechanistic and in vivo investigations.

Stability Study

Table 4 presents the results of the stability evaluation of the optimized luteolin-loaded niosomal dispersion. Throughout the three-month study period, no statistically significant changes were observed in particle size,

Table 4 Stability evaluation of optimized luteolin-loaded Niosomal dispersion

Storage condition	Appearance	Particle size (nm)	PDI	Zeta potential (mV)	Entrapment efficiency (%)
Initial	Milky white	162.67 ± 2.87	0.173 ± 0.01	−34.63 ± 1.07	87.07 ± 1.69
Refrigerated (4 °C ± 2 °C)					
1 month	Milky white	167.38 ± 1.17	0.201 ± 0.01	−32.63 ± 2.17	85.70 ± 1.32
3 months	Milky white	170.54 ± 1.82	0.175 ± 0.02	−33.63 ± 2.1	84.22 ± 2.44
Accelerated (40 °C ± 2 °C/75% ± 5% RH)					
1 month	Milky white	159.69 ± 2.97	0.169 ± 0.02	−31.63 ± 1.74	84.23 ± 2.65
3 months	Milky white	169.47 ± 2.48	0.182 ± 0.01	−30.63 ± 2.11	82.56 ± 2.34

Data expressed as mean ± SD, n = 3

PDI, zeta potential and entrapment efficiency under both refrigerated and accelerated storage conditions. These findings indicate that the formulation maintained its physicochemical stability over time. Furthermore, the consistent appearance of the niosomal dispersion with no signs of degradation or incompatibility, suggests that luteolin-loaded niosomes were stable and compatible with the selected excipients. Overall, the results confirm the robustness and stability of the optimized formulation under the tested ICH-recommended storage conditions.

Conclusion

The present study successfully formulated and optimized luteolin-loaded niosomes using a central composite design to improve the therapeutic potential of luteolin against breast cancer. The nanocarriers exhibited favorable physicochemical properties, including uniform particle size, high entrapment efficiency, and sustained drug release. Structural analyses confirmed successful encapsulation with a transition of luteolin to an amorphous form, suggesting enhanced solubility. In vitro cytotoxicity studies demonstrated that the niosomal formulation significantly outperformed free luteolin in inhibiting MCF-7 cell proliferation, likely due to improved cellular uptake. These findings are consistent with previously reported mechanisms of luteolin action, such as apoptosis induction, ROS regulation, and inhibition of oncogenic kinases; however, direct mechanistic validation was not performed in this study and remains a limitation. Importantly, the absence of in vivo pharmacokinetic and therapeutic evaluation also restricts the translational relevance of the current findings. Future work will therefore focus on conducting comprehensive in vivo studies, including mechanistic assays, systemic pharmacokinetics, and therapeutic efficacy, to confirm the potential of luteolin-loaded niosomes. Overall, this study provides a strong foundation for further preclinical development of luteolin-loaded niosomes as a promising, biocompatible strategy for breast cancer management.

Supplementary Information The online version contains supplementary material available at https://doi.org/10.1007/s12247-025-10348-2.

Author Contributions CRediT authorship contribution statement Nikhil Girase: Literature review, writing original draft, reviewing, and editing. Rakesh Daude: Literature review, writing original draft, reviewing, and editing. Kailas Moravkar: Literature review, writing original draft, editing, Supervision and Project administration. Shailesh Chalikwar: Supervision, Project administration. Ganesh Shevalkar: Conceptualization, Supervision, Reviewing, and Editing. Bhushan Bhairav: Conceptualization, Supervision, Reviewing, and Editing.

Data Availability No datasets were generated or analysed during the current study.

Declarations

Competing Interests The authors declare no competing interests.

References

1. Ansari MJ, Alshetaili A, Aldayel IA, Alablan FM, Alsulays B, Alshahrani S, et al. Formulation, characterization, in vitro and in vivo evaluations of self-nanoemulsifying drug delivery system of luteolin. J Taibah Univ Sci. 2020;14:1386–401.
2. Chen Z, Kong S, Song F, Li L, Jiang H. Pharmacokinetic study of luteolin, apigenin, chrysoeriol and diosmetin after oral administration of *Flos chrysanthemi* extract in rats. Fitoterapia. 2012;83:1616–22.
3. Marianecci C, Rinaldi F, Mastriota M, Pieretti S, Trapasso E, Paolino D, et al. Anti-inflammatory activity of novel ammonium glycyrrhizinate/niosomes delivery system: human and murine models. J Control Release. 2012;164:17–25.
4. Wang H, Luo Y, Qiao T, Wu Z, Huang Z. Luteolin sensitizes the antitumor effect of cisplatin in drug-resistant ovarian cancer via induction of apoptosis and inhibition of cell migration and invasion. J Ovarian Res. 2018;11:93.
5. Luo Y, Chen S, Zhou J, Chen J, Tian L, Gao W, et al. Luteolin cocrystals: characterization, evaluation of solubility, oral bioavailability and theoretical calculation. J Drug Deliv Sci Technol. 2019;50:248–54.
6. Lv J, Song X, Luo Z, Huang D, Xiao L, Zou K. Luteolin: exploring its therapeutic potential and molecular mechanisms in pulmonary diseases. Front Pharmacol. 2025. https://doi.org/10.3389/fphar.2025.1535555.
7. Dang H, Meng MHW, Zhao H, Iqbal J, Dai R, Deng Y, et al. Luteolin-loaded solid lipid nanoparticles synthesis, characterization, & improvement of bioavailability, pharmacokinetics in vitro and vivo studies. J Nanopart Res. 2014;16:2347.
8. Alshehri S, Imam SS, Altamimi MA, Hussain A, Shakeel F, Elzayat E, et al. Enhanced dissolution of Luteolin by solid dispersion prepared by different methods: physicochemical characterization and antioxidant activity. ACS Omega. 2020;5:6461–71.
9. Zhang N, Zhang F, Xu S, Yun K, Wu W, Pan W. Formulation and evaluation of luteolin supersaturatable self-nanoemulsifying drug delivery system (S-SNEDDS) for enhanced oral bioavailability. J Drug Deliv Sci Technol. 2020;58:101783.
10. Shin K, Choi H, Song SK, Yu JW, Lee JY, Choi EJ, et al. Nanoemulsion vehicles as carriers for follicular delivery of Luteolin. ACS Biomater Sci Eng. 2018;4:acsbiomaterials.8b00220.
11. Liu B, Li W, Zhao J, Liu Y, Zhu X, Liang G. Physicochemical characterisation of the supramolecular structure of luteolin/cyclodextrin inclusion complex. Food Chem. 2013;141:900–6.
12. Hou X, Sheng JJ. Properties, preparation, stability of nanoemulsions, their improving oil recovery mechanisms, and challenges for oil field applications—a critical review. Geoenergy Science and Engineering. 2023;221:211360.
13. Dhondale MR, Thakor P, Nambiar AG, Singh M, Agrawal AK, Shastri NR, et al. Co-crystallization approach to enhance the stability of moisture-sensitive drugs. Pharmaceutics. 2023;15:189.
14. Mishra V, Bansal KK, Verma A, Yadav N, Thakur S, Sudhakar K, et al. Solid lipid nanoparticles: emerging colloidal nano drug delivery systems. Pharmaceutics. 2018;10:191.
15. Shevalkar G, Vavia P. Solidified nanostructured lipid carrier (S-NLC) for enhancing the oral bioavailability of ezetimibe. J Drug Deliv Sci Technol. 2019;53:101211.
16. Fouda-Mbanga BG, Tywabi-Ngeva Z, Badawy WM, Ebite C, Onotu OP, Abogidi C, et al. Green cyclodextrins-derivatives for

sustainable remediation of pesticides and heavy metals: a review. J Mol Struct. 2025;1328:141326.
17. Darandale SS, Shevalkar GB, Vavia PR. Effect of lipid composition in Propofol formulations: decisive component in reducing the free Propofol content and improving pharmacodynamic profiles. AAPS PharmSciTech. 2017;18:441–50.
18. Pawar S, Shevalkar G, Vavia P. Glucosamine-anchored doxorubicin-loaded targeted nano-niosomes: pharmacokinetic, toxicity and pharmacodynamic evaluation. J Drug Target. 2016;24:730–43.
19. Bartelds R, Nematollahi MH, Pols T, Stuart MCA, Pardakhty A, Asadikaram G et al. Z <>Leonenko editor 2018 Niosomes, an alternative for liposomal delivery. PLoS ONE 13 1–18.
20. Said AR, Arafa MF, El-Dakroury WA, Alshehri S, El Maghraby GM. Bilosomes and niosomes for enhanced intestinal absorption and in vivo efficacy of cytarabine in treatment of acute myeloid leukemia. Pharmaceuticals. 2024;17:1572.
21. Fardpour M, Falahi Robattorki F, Sarabi H, Zarazvand F, Arvand S, Saegh A. Enhanced therapeutic potential of Paclitaxel-loaded niosomes on ovarian cancer cell line. Asian Pac J Cancer Biol. 2025;10:71–7.
22. Jadon PS, Gajbhiye V, Jadon RS, Gajbhiye KR, Ganesh N. Enhanced oral bioavailability of Griseofulvin via niosomes. AAPS PharmSciTech. 2009;10:1186.
23. Ag Seleci D, Seleci M, Walter J-G, Stahl F, Scheper T. Niosomes as nanoparticular drug carriers: fundamentals and recent applications. J Nanomater. 2016;2016:1–13.
24. Chen S, Hanning S, Falconer J, Locke M, Wen J. Recent advances in non-ionic surfactant vesicles (niosomes): fabrication, characterization, pharmaceutical and cosmetic applications. Eur J Pharm Biopharm. 2019;144:18–39.
25. Nunse D, Shevalkar GB, Borse L. Innovative polymeric micelles with In-Situ gelation for enhanced ocular delivery of ketoconazole. J Pharm Innov. 2025;20:1–12.
26. Abidin L, Mujeeb M, Imam SS, Aqil M, Khurana D. Enhanced transdermal delivery of Luteolin via non-ionic surfactant-based vesicle: quality evaluation and anti-arthritic assessment. Drug Deliv. 2016;23:1069–74.
27. Rise Desnita H, Nur Hichmah SL, Desnita R, Hichmah HN, Luliana S. Effect of surfactant concentration on the entrapment efficiency niosomes aqueous extract of cassava leaves (Manihot esculenta Crantz). Asian J Pharm. 2019;13:276–81.
28. Kovačević AB, Müller RH, Keck CM. Formulation development of lipid nanoparticles: improved lipid screening and development of tacrolimus loaded nanostructured lipid carriers (NLC). Int J Pharm. 2020;576:118918.
29. Chauhan MK, Bhatt N. Bioavailability enhancement of polymyxin B with novel drug delivery: development and optimization using quality-by-design approach. J Pharm Sci. 2019;108:1521–8.
30. Mohanty D, Rani MJ, Haque MA, Bakshi V, Jahangir MA, Imam SS, et al. Preparation and evaluation of transdermal naproxen niosomes: formulation optimization to preclinical anti-inflammatory assessment on murine model. J Liposome Res. 2020;30:377–87.
31. Sheena TV, Jyothish B, Jacob J. Preparation, characterization, and in vitro evaluation of the anticancer activity of Ce3+doped CuFe2O4 spinel nanoparticles in MCF-7 cell lines. Chem Phys Impact. 2024;8:100423.
32. Monem AS, Ghannam MM, ElBaz TA, Fahmy HM. Synthesis, characterization, and cytotoxicity evaluation of magnetoliposomes in human breast cancer MCF-7 cells. Biochem Biophys Res Commun. 2025;772:152016.
33. Ma J, Pan Z, Du H, Chen X, Zhu X, Hao W, et al. Luteolin induces apoptosis by impairing mitochondrial function and targeting the intrinsic apoptosis pathway in gastric cancer cells. Oncol Lett. 2023;26:327.
34. Bhargav E, Mohammed N, Singh UN, Ramalingam P, Challa RR, Vallamkonda B, et al. A central composite design-based targeted quercetin nanoliposomal formulation: optimization and cytotoxic studies on MCF-7 breast cancer cell lines. Heliyon. 2024;10:e37430.
35. Mawazi SM, Ge Y, Widodo RT. Niosome preparation techniques and structure—an illustrated review. Pharmaceutics. 2025. https://doi.org/10.3390/pharmaceutics17010067.
36. Kumar GP, Rajeshwarrao P. Nonionic surfactant vesicular systems for effective drug delivery—an overview. Acta Pharm Sin B. 2011;1:208–19.
37. Khoee S, Yaghoobian M. Niosomes: a novel approach in modern drug delivery systems. In: Nanostructures Drug Deliv. Elsevier Inc.; 2017.
38. Shevalkar G, Pawar M, Vavia P. Nanostructured lipid carriers (NLCs) of lumefantrine with enhanced permeation. J Pharm Innov. 2022;17:1221–34.
39. Shevalkar G, Pai R, Vavia P. Nanostructured lipid carrier of propofol: a promising alternative to marketed soybean oil–based nanoemulsion. AAPS PharmSciTech. 2019;20:201.
40. Shevalkar G, Borse L. Self-microemulsifying drug delivery system (SMEDDS) for oral delivery of zafirlukast: design, formulation, and pharmacokinetic evaluation. J Drug Deliv Sci Technol. 2024;101:106298.
41. Goyal G, Garg T, Malik B, Chauhan G, Rath G, Goyal AK. Development and characterization of niosomal gel for topical delivery of benzoyl peroxide. Drug Deliv. 2015;22:1027–42.
42. Mali N, Darandale S, Vavia P. Niosomes as a vesicular carrier for topical administration of minoxidil: formulation and in vitro assessment. Drug Deliv Transl Res. 2013;3:587–92.
43. Shevalkar G, Pote S, Rathod S, Suryawanshi M. Thiocolchicoside niosomal gel: design-driven optimization for superior skin permeation. J Pharm Innov. 2025;20:1–17.
44. Kumbhar D, Wavikar P, Vavia P. Niosomal gel of lornoxicam for topical delivery: in vitro assessment and pharmacodynamic activity. AAPS PharmSciTech. 2013;14:1072–82.
45. Akbari J, Saeedi M, Morteza-Semnani K, Hashemi SMH, Babaei A, Eghbali M, et al. Innovative topical niosomal gel formulation containing diclofenac sodium (niofenac). J Drug Target. 2022;30:108–17.
46. Lee S, Seo D-H, Park H-L, Choi Y, Jung S. Solubility enhancement of a hydrophobic flavonoid, Luteolin by the complexation with cyclosophoraoses isolated from rhizobium meliloti. Antonie Van Leeuwenhoek. 2003;84:201–7.
47. Zaid Alkilani A, Hamed R, Abdo H, Swellmeen L, Basheer HA, Wahdan W, et al. Formulation and evaluation of Azithromycin-Loaded Niosomal gel: optimization, in vitro studies, rheological characterization, and cytotoxicity study. ACS Omega. 2022;7:39782–93.
48. Pandey P, Pal R, Khadam VKR, Chawra HS, Singh RP. Advancement and characteristics of non-ionic surfactant vesicles (Niosome) and their application for analgesics. Int J Pharm Investig. 2024;14:616–32.
49. Jain N, Verma A, Jain N. Formulation and investigation of pilocarpine hydrochloride Niosomal gels for the treatment of glaucoma: intraocular pressure measurement in white albino rabbits. Drug Deliv. 2020;27:888–99.
50. Hemmati J, Chegini Z, Arabestani MR. Niosomal-based drug delivery platforms: A promising therapeutic approach to fight staphylococcus aureus drug resistance. Huang Z, editor. J Nanomater. 2023;2023:1–18.
51. Bari D, Das U, Shevalkar G, Kapadia R, Singhai V, Pardeshi C. Advancements in Brain Lymphatic System and Its Involvement in Neurological Diseases. In: Adv Target Lymphat Syst. Cham: Springer Nature Switzerland; 2024. p. 23–51.
52. Imran M, Rauf A, Abu-Izneid T, Nadeem M, Shariati MA, Khan IA, et al. Luteolin, a flavonoid, as an anticancer agent: a review. Biomed Pharmacother. 2019;112:108612.

53. Barani M, Mirzaei M, Torkzadeh-Mahani M, Adeli-sardou M. Evaluation of *carum*-loaded niosomes on breast cancer cells: physicochemical properties, in vitro cytotoxicity, flow cytometric, DNA fragmentation and cell migration assay. Sci Rep. 2019;9:7139.
54. Barani M, Mirzaei M, Torkzadeh-Mahani M, Nematollahi MH. Lawsone-loaded niosome and its antitumor activity in MCF-7 breast cancer cell line: a nano-herbal treatment for cancer. DARU J Pharm Sci. 2018;26:11–7.
55. Cook MT, Mafuvadze B, Besch-Williford C, Ellersieck MR, Goyette S, Hyder SM. Luteolin suppresses development of medroxyprogesterone acetate-accelerated 7,12-dimethylbenz(a) anthracene-induced mammary tumors in Sprague-Dawley rats. Oncol Rep. 2016;35:825–32.
56. Lim DY, Jeong Y, Tyner AL, Park JHY. Induction of cell cycle arrest and apoptosis in HT-29 human colon cancer cells by the dietary compound luteolin. Am J Physiol Liver Physiol. 2007;292:G66-75.
57. Eugster R, Luciani P. Liposomes: bridging the gap from lab to pharmaceuticals. Curr Opin Colloid Interface Sci. 2025;75:101875.
58. Xuan L, Ju Z, Skonieczna M, Zhou P, Huang R. Nanoparticles-induced potential toxicity on human health: applications, toxicity mechanisms, and evaluation models. MedComm. 2023. https://doi.org/10.1002/mco2.327.
59. Ghezzi M, Pescina S, Padula C, Santi P, Del Favero E, Cantù L, et al. Polymeric micelles in drug delivery: an insight of the techniques for their characterization and assessment in biorelevant conditions. J Control Release. 2021;332:312–36.
60. Janaszewska A, Lazniewska J, Trzepiński P, Marcinkowska M, Klajnert-Maculewicz B. Cytotoxicity of dendrimers. Biomolecules. 2019;9:330.
61. Shevalkar GB, Yadav NR, Pardeshi CV, Surana SJ. Advanced drug delivery systems for glioblastoma. Adv Drug Deliv Syst Manag Cancer. Elsevier; 2021. pp. 183–95.